Quantifying background magnetic-field inhomogeneity for improved interpretation of free induction decay measurements

Denys Grombacher[1], Jan O. Walbrecker[1], and Rosemary Knight[1]

ABSTRACT

Nuclear magnetic resonance measurements provide useful insight into pore-scale properties of porous media. One influence affecting the measurement is inhomogeneity in the static background magnetic field (B_0). This inhomogeneity can significantly alter the relaxation signal and potentially obscure pore-scale information. To improve the understanding of this effect on the free-induction decay (FID), a measurement still commonly used in practice, a novel methodology is developed to estimate the statistical distribution of B_0. A suite of preparatory pulse sequences is developed to encode information about the B_0 field in the initial amplitude and phase of the FID following each sequence and an inversion is employed to predict the statistical distribution of B_0. Knowledge of the B_0 distribution is then used to correct for the impact of B_0 inhomogeneity on the FID measurement; this is essential for improving the usefulness of FID measurements for the estimation of pore-scale properties. Results are presented for both numerical and laboratory studies verifying the feasibility of the developed methodology in a controlled laboratory environment, and demonstrating that knowledge of the statistical distribution of B_0 is sufficient to estimate the impact of B_0 inhomogeneity on the FID in cases where B_0 inhomogeneity causes less than an order of magnitude decrease in the relaxation times governing the FID.

INTRODUCTION

The growing dependence of many populations on groundwater demands improvements in techniques that can quantify the volume of producible groundwater, and provide information needed for the development of sustainable management strategies. The nuclear magnetic resonance (NMR) method is a powerful geophysical technique for aquifer characterization using logging and surface-based methods, with the distinct advantage of providing direct sensitivity to water content.

The NMR technique exploits the nuclear spin magnetic moment (spin) of the hydrogen nuclei contained in water molecules. In a background magnetic field (B_0), these spins tend to preferentially align along the B_0-direction, resulting in the formation of a net magnetization. The NMR experiment involves perturbing this magnetization through the application of a secondary magnetic field (B_1) and the subsequent monitoring of its return to equilibrium. The amplitude of the measured signal gives insight into water content (equal to porosity in saturated material), while the signal decay contains the information about the pore-scale geometry desired for aquifer characterization.

The simplest experiment involves measuring the voltage induced by the magnetization after a single perturbing B_1 pulse, called a free-induction decay (FID). The FID is controlled by the relaxation time T_2*. The problem with T_2* is that it may be significantly affected by B_0 inhomogeneity (Bloom, 1955), which occurs naturally due to magnetic susceptibility contrasts in the subsurface (Hurlimann, 1998). In some cases, the impact of B_0 inhomogeneity is so dominant that T_2* loses its connection to the pore geometry (Grunewald and Knight, 2012), and thus has limited value for aquifer characterization.

Techniques such as the spin-echo (Hahn, 1950) or CPMG (named after the authors; Carr and Purcell, 1954; Meiboom and Gill, 1958) and inversion-recovery (Callaghan, 1991) pulse sequences may be used to reduce or eliminate the affect of B_0 inhomogeneity. This results in the measurement of the relaxation time T_2 or T_1, respectively, both of which are closely tied to pore-scale geometry. NMR-logging measurements of T_2 are widely used in the petroleum industry to estimate properties such as pore size and permeability (Seevers, 1966; Timur, 1968; Kenyon, 1988; Coates, 1991), and more recently used to obtain estimates of hydraulic conductivity in unconsolidated aquifers (Dlubac et al., 2013; Walsh et al., 2013). However, for the surface NMR technique (Legchenko

and Sushakov, 1998; Legchenko and Valla, 2002), use of the FID to measure T_2* remains common because it provides a fast measurement with a high-density time sampling and the ability to measure the fastest relaxation times, compared with techniques to measure T_2 or T_1 directly. A methodology designed to complement the FID measurement and address its heightened sensitivity to B_0 inhomogeneity could therefore exploit these advantageous features while potentially improving the FID's utility for the estimation of pore-scale properties. We present a proof of concept study in a controlled laboratory environment demonstrating a novel methodology to characterize the influence of B_0 inhomogeneity on FID measurements, addressing a major concern with FID measurements. The hypothesis we wish to test is: By quantifying the statistical distribution of B_0 we can correct for the impact of B_0 inhomogeneity on T_2*.

We test this hypothesis by conducting a series of laboratory experiments on water samples doped with $FeSO_4$. By studying samples of varying concentrations of $FeSO_4$, the relative impact of B_0 inhomogeneity on T_2* is different for each sample. As all samples are liquid and are measured with the same laboratory instrument, we can presume that the statistical distribution of B_0 will remain constant, thus providing a simple system for testing of our hypothesis. To quantify the statistical distribution of B_0, we develop a novel methodology using a preparatory pulse sequence, consisting of two pulses separated by a delay time, to encode information about B_0 inhomogeneity in the amplitude and phase of the following FID. We invert the FID amplitudes and phases measured after a suite of preparatory sequences to obtain an estimate of the statistical distribution of B_0, and quantify its impact on the FID. A key difference between this methodology and other techniques used to characterize B_0 (Hurlimann, 1998; Sun and Dunn, 2002) is that this method estimates the magnitudes of B_0 and not gradients in B_0. Knowledge of the gradients in B_0 is essential for characterizing the influence of B_0 inhomogeneity in the spin-echo and CPMG pulse sequences, but as we are concerned with the FID, knowledge of the statistical distribution is necessary. A comparison between relaxation times estimated after correcting T_2* for the impact of B_0 heterogeneity and T_2 is presented to demonstrate that knowledge of the statistical distribution of B_0 is sufficient to correct for the impact of B_0 inhomogeneity on the FID.

BACKGROUND

Effect of inhomogeneous B_0 on relaxation

In this article, we treat the dynamics of the magnetization classically, which allows us to represent the magnetization originating from an ensemble of spins as a single vector **M**. The return of the magnetization **M** to equilibrium following perturbation by a B_1 pulse (called relaxation) involves the decay of the transverse magnetization (the component transverse to the B_0-direction) and the regrowth of the longitudinal magnetization (the component parallel to the B_0-direction). The decay and regrowth are modeled as exponential processes each controlled by different time constants: T_2 controls the relaxation of the transverse component and T_1 the longitudinal component. As the transverse component decays, it precesses about the B_0 direction at the Larmor frequency, ω_0, which depends on the magnitude of the B_0 field and the gyromagnetic ratio $\gamma(|\omega_0| = |\gamma B_0|)$. The precession allows the magnitude of the transverse component to be measured inductively using a coil.

In a homogeneous B_0 field, regardless of the data acquisition technique used (spin-echo, CPMG, FID), the decay of the transverse component is controlled by T_2. This term is affected by bulk relaxation of spins contained in the fluid (Slichter, 1980) and surface relaxation occurring due to interactions between spins and the grain boundaries (Brownstein and Tarr, 1979). In practice, it is often assumed that the T_2 relaxation is dominated by surface relaxation. In this limit, called the fast-diffusion limit, T_2 is given by equation 1 (Cohen and Mendelsen, 1982):

$$\frac{1}{T_2} = \rho \frac{S}{V}, \qquad (1)$$

where ρ is called the surface relaxivity, a parameter governing the ability of the grain surface to promote relaxation (Brownstein and Tarr, 1979; Godefroy et al., 2001). The S/V term is the surface-area-to-volume ratio of the pore space, which provides the link between relaxation times and pore geometry.

In an inhomogeneous B_0 field, which occurs naturally due to magnetic susceptibility contrasts in the subsurface (Hurlimann, 1998), this link to S/V is complicated by the presence of an additional mechanism that accelerates the measured decay (Hahn, 1950). Spins at different spatial locations are subject to different magnitudes of the B_0 field and therefore precess at different Larmor frequencies. As time progresses, the spins accumulate different phase shifts and the resulting dephasing enhances the decay. When no attempt to mitigate this dephasing is made, such as in the FID measurement, the decay is described by the effective relaxation time T_2*,

$$\frac{1}{T_2*} = \frac{1}{T_2} + \frac{1}{T_{2IH}}. \qquad (2)$$

The T_{2IH} term describes all signal loss related to B_0 inhomogeneity. It depends on the statistical distribution of B_0 experienced by the spins during the course of the NMR experiment. To illustrate how T_{2IH} can impact the relationship between T_2* and pore size, consider Figure 1, which summarizes the results of Figure 4 in Grunewald and Knight (2012). At low susceptibilities (~5 10^{-6} cgs, eg., quartz), corresponding to weak T_{2IH}, T_2* approximates T_2 well over a wide range of pore sizes, providing a strong connection to pore size. At medium susceptibilities (~100 × 10^{-6} cgs, pyrite) T_2* only approximates T_2 over a limited range of pore sizes. As such, at large pore sizes (small S/V) the influence of T_{2IH} results in T_2* not being reflective of pore size. At higher susceptibilities (~1000 × 10^{-6} cgs, hematite), T_{2IH} becomes dominant and T_2* is no longer a good indicator of pore size. This highlights that it is the relative magnitudes of T_{2IH} and T_2 that determine whether or not T_2* is a good indicator of pore size.

To quantify the potential impact of T_{2IH} on T_2*, consider an example of a soil containing 0.1% magnetite. We estimate the bulk susceptibility of this soil to be ~200 × 10^{-6} cgs using the empirical relationship $k = 0.0026 * V^{1.11}$ (Grant and West, 1965), where k is the magnetic susceptibility (cgs) and V is the volume percent of magnetite. The B_0 bandwidth (at Earth's field, where $B_0 \sim 2\,\text{kHz}$) due to the susceptibility contrast between the 0.1% magnetite soil and water can be approximated to be 1.5 Hz, corresponding to a T_{2IH} of roughly 210 ms (Chen et al., 2005). Given typical T_2 values of 50, 100, 200, and 300 ms, when combined with a T_{2IH} of this magnitude (210 ms) equation 2 states that T_2* would

underestimate T_2 by 19%, 32%, 49%, and 59% in each case. This magnitude of discrepancy could lead to significantly underestimated pore sizes and permeability despite the seemingly narrow B_0 bandwidth. Several field studies have noted this bias, where T_2* has been observed to underestimate T_2 (Muller et al., 2005; Plata and Rubio, 2008; Roy et al., 2008). Furthermore, as the B_0 bandwidth increases, T_{2IH} also increases and the underestimation will be even greater. We therefore require an understanding of the B_0 field before we can use T_2* to infer pore geometry (S/V) information.

When the FID is modeled in the time domain as an exponential decay controlled by the relaxation time T_2*, it is implicitly assumed that the statistical distribution of B_0 is Lorentzian because the Fourier transform of a Lorentzian distribution (which describes the dephasing) is an exponential function. In the case of an arbitrary B_0 distribution, the FID is described by equation 3 (Yablonskiy and Haacke, 1994; Grunewald and Knight, 2011):

$$M(t) = M_0 h(t) e^{-t/T_2},\qquad(3)$$

where $M(t)$ and M_0 are the amplitude at time t and the initial amplitude of the FID, respectively. The $h(t)$ function describes the dephasing due to B_0 inhomogeneity. The exponential term (controlled by T_2) describes the decay that would occur given a homogeneous B_0. Equation 3 is valid when diffusion is neglected, but remains an appropriate approximation for the case where the length scale of B_0 variation is larger than the diffusion length. In this limit, $h(t)$ is the Fourier transform of the statistical distribution of B_0 (Yablonskiy and Haacke, 1994). Unless B_0 is characterized, $h(t)$ remains an unknown and the connection to pore geometry unclear.

Effect of inhomogeneous B_0 on excitation

In addition to impacting the measured decay rate, B_0 inhomogeneity affects the ability of the applied B_1 pulse to perturb the magnetization due to a mechanism called off-resonance effects (Walbrecker et al., 2011). Off-resonance effects occur due to an offset between the Larmor frequency, ω_0, and the frequency of the applied B_1 field, ω. To illustrate this effect, it is beneficial to consider the excitation process in a reference frame rotating at ω. In this frame, the effective magnetic field during excitation B_{eff} is given by equation 4 (Levitt, 2006):

$$B_{\text{eff}} = \left(B_0 - \frac{\omega}{\gamma}\right)\hat{\mathbf{z}} + B_1\hat{\mathbf{x}},\qquad(4)$$

where we have oriented the rotating frame with the z-direction along B_0. The phase of the B_1 pulse determines its orientation in the rotating frame; here, we align the frame so a B_1 pulse of phase zero points in the x-direction, such as given in equation 4. The B_{eff} field induces a torque on the magnetization, $\mathbf{M}$, leading to the nutation of $\mathbf{M}$ about the B_{eff} axis, at a rate proportional to the magnitude of B_{eff}. In the on-resonance situation ($\omega = \omega_0$), the z-component of B_{eff} vanishes ($B_0 - \omega/\gamma = 0$). In this case, B_{eff} is equal to the applied B_1. This induces a nutation of $\mathbf{M}$ (in the rotating frame) through a flip angle $\theta = \gamma B_1 \tau$ about an axis oriented along B_1; where τ is the length of the B_1 pulse. Experimental control of the duration and phase of B_1 allows the angle through which $\mathbf{M}$ is rotated and the orientation of the rotation axis, respectively, to be manipulated precisely. If the excitation is off resonance ($\omega \neq \omega_0$), there remains a residual z-component to B_{eff} ($B_0 - \omega/\gamma \neq 0$ in equation 4).

To demonstrate the impact of off-resonance effects, consider Figure 2, which shows on-resonance and off-resonance excitation due to a nominal $\pi/2_{-x}$ pulse, respectively. Note that the subscript denotes the axis along which B_1 is oriented in the rotating frame and $\pi/2$ the flip angle. All rotations in this study are left handed. The on-resonance $\pi/2_{-x}$ pulse (red line) results in a rotation of $\mathbf{M}$ into the transverse plane, whereas the off-resonance pulse (blue line, with $\omega_0 = 2.2$ MHz, $\omega_0 - \omega = 2$ kHz, and $\tau = 21.6$ μs) leaves $\mathbf{M}$ with a residual longitudinal component and a transverse compo-
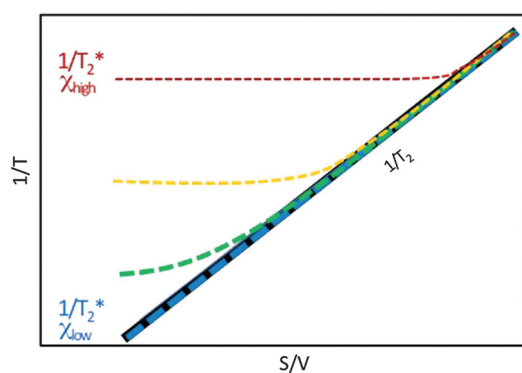

Figure 1. Schematic illustration of the difference in the relationship with S/V of the NMR parameters T_2 and T_2*. Pore size is presumed to be inversely proportional to S/V. When surface relaxation dominates, T_2 exhibits a linear dependence on S/V. Increasing magnetic susceptibility is shown as increasing warmth in color. At low levels of magnetic susceptibility (shown in blue), T_2 and T_2* exhibit the same linear relationship with S/V. As magnetic susceptibility increases and/or S/V decreases (pore size increases), the dependence of T_2* on S/V is increasingly masked due to relaxation associated with the impacts of an inhomogeneous magnetic field; i.e., T_{2IH}.
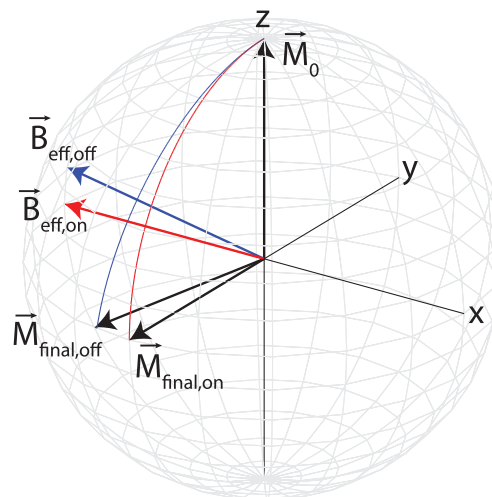

Figure 2. Induced spin dynamics during a nominal $\pi/2_{-x}$ pulse for an on-resonance ($\omega = \omega_0$) and an off-resonance ($\omega \neq \omega_0$) case. The induced rotations are shown in the rotating reference frame, and are left handed. Black arrows show the initial ($\mathbf{M}_0$) and final ($\mathbf{M}_{\text{final}}$) magnetizations before and after the pulse. Red and blue arrows show the B_{eff} axis for the on-resonance and off-resonance cases, respectively. The thin red and thin blue lines illustrate the magnetization's trajectory during the on-resonance and off-resonance pulse, respectively.

nent oriented in a different direction (not in the y-z plane). This manifests as a variation in transverse magnetization's amplitude and phase. Of interest in this study is the impact on the magnetization's transverse component (phase and amplitude), as the extent to which off-resonance effects are observed may reveal information about B_0 inhomogeneity.

METHODOLOGY

We present a novel methodology consisting of four steps to test the hypothesis that knowledge of the statistical distribution of B_0 may be used to compensate for the impact of B_0 inhomogeneity on T_2*. The workflow is described in Figure 3. The first three steps focus on quantifying the statistical distribution of B_0, whereas the final step estimates and corrects for the impact of B_0 inhomogeneity on the FID.

Preparatory pulse sequence design and measurement

The preparatory pulse sequences used in this study are similar in concept to composite pulses (Freeman, 1980; Levitt, 1986). Composite pulses, consisting of a collection of pulses applied in quick succession, were originally designed to counter off-resonance effects. In contrast, we design preparatory sequences to exploit off-resonance effects and dephasing to investigate the B_0 field.

To illustrate this concept, consider the following two preparatory sequences. The first consists of two $\pi/2$ pulses separated by delay time $\tau_d = 450$ μs, where the first and second $\pi/2$ pulses rotate **M** about the $-x$- and y-axes, respectively. This sequence is denoted as a $\pi/2_{-x} - \tau_d - \pi/2_y$. The induced spin dynamics for a range of offsets with $\omega_0 = [\omega - 500 \text{ Hz}, \omega + 500 \text{ Hz}]$, with $\omega = 2$ MHz, and $\tau = 21.6$ μs are illustrated in Figure 4. The initial $\pi/2_{-x}$ pulse rotates the spins from their equilibrium state along z toward the transverse plane (Figure 4a). During the delay time τ_d, the spins dephase according to their local offset frequency $\Delta\omega(\Delta\omega = \omega_0 - \omega)$, resulting in them fanning out in the transverse plane (Figure 4b). Spins with $\omega_0 > \omega$ rotate clockwise in the rotating frame, whereas spins with $\omega_0 < \omega$ rotate counterclockwise. Next, the $\pi/2_y$ pulse rotates spins at large offsets out of the transverse plane giving them a large z-component (Figure 4c). On-resonance spins ($\Delta\omega \approx 0$, green in Figure 4c) are not rotated by the $\pi/2_y$

pulse because they are oriented along the rotation axis. Figure 4d highlights the spins that have the largest contributions to the measured FID (i.e., largest transverse components), identified as those lying closest to the perimeter of the unit circle. Therefore, the FID amplitude following this first preparatory sequence, determined by the sum of all transverse components, allows us to comment on the abundance of spins with ω_0 on or near resonance.

The second preparatory sequence is very similar, consisting of a $\pi/2_{-x} - \tau_d - \pi/2_x$ sequence. Only the phase of the second $\pi/2$ pulse is changed, causing it to induce a rotation about the $+x$ axis instead of the $+y$ axis. This sequence again begins with a $\pi/2_{-x}$ pulse (Figure 4a) and a delay time τ_d, during which the spins fan out in the transverse plane (Figure 4b). The second $\pi/2$ pulse induces a rotation about the $+x$ axis (Figure 4e). Spins with $\omega_0 \approx \omega$ are left with large z-components, and correspondingly small transverse components. For spins at large offsets, the accumulated phases during τ_d reduce the ability of the $\pi/2_x$ pulse to return them to the z-direction. Figure 4f demonstrates that spins at offsets of ≈ 500 Hz (blue and red in Figure 4f) are left with the largest transverse components. In contrast to the previous example, the FID amplitude here is primarily determined by the number of spins at large offsets. Despite the fact that these two preparatory sequences are identical except for the phase of the second pulse, the net perturbation is very different. It is this difference in the net perturbation that allows information about the statistical distribution of B_0 to be encoded in the FID amplitude and phase following each preparatory sequence.

These two examples highlight the concept behind the developed methodology to determine the B_0 distribution. Each preparatory sequence is designed to have sensitivity to different regions of the B_0 distribution (from on to far off resonance). The timing diagram for the developed preparatory sequences is shown in Figure 5. Each preparatory pulse is defined by four parameters: the duration of pulse 1 τ_1, the delay time τ_d, the duration of pulse 2 τ_2, and the relative phase Φ between the pulses. Varying these parameters gives a different sensitivity to B_0 inhomogeneity. The preparatory
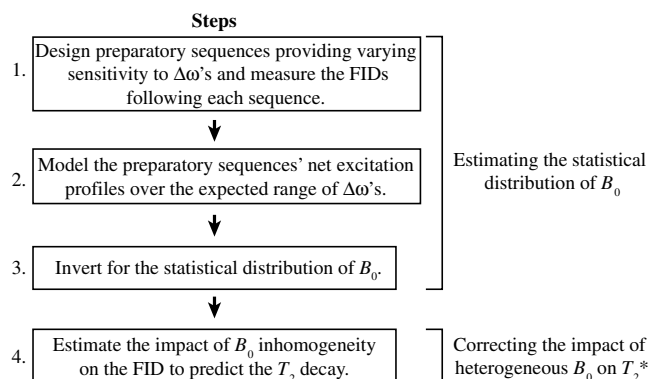

Figure 3. Flow chart demonstrating the workflow of the proposed methodology. Steps 1, 2, and 3 are focused on estimating the statistical distribution of B_0. Step 4 focuses on estimating the impact of B_0 inhomogeneity on T_2*.
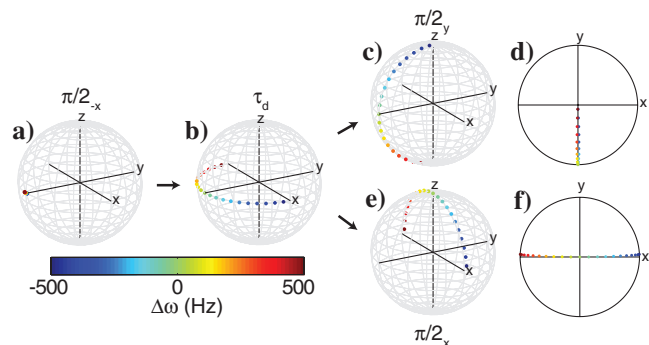

Figure 4. Spin dynamics during two preparatory pulse sequences for a range of frequency offsets ± 500 Hz about ω (color coded) in a static B_0 field of 2 MHz. (a) Initial magnetization along z (not shown) is rotated onto the transverse plane along $-y$ by the first pulse $\pi/2_{-x}$. (b) During the delay time of 450 μs, spins fan out in the transverse plane by an angle that is determined by its offset, $\varphi = \Delta\omega\tau_d$. (c) The final excitation profile after the second pulse for the $\pi/2_{-x} - \tau - \pi/2_y$ preparatory sequence. (d) Projection of (c) into the transverse plane. (e) The final excitation profile after second pulse for the $\pi/2_{-x} - \tau - \pi/2_x$ preparatory sequence. (f) Projection of (e) into the transverse plane. All pulse lengths are 21.6 μs.

sequences used in this study are listed in Table 1. They are restricted to only two individual pulses for simplicity. In principle, they may consist of many individual pulses. Figure 6 illustrates the net excitation profile (transverse plane) for all preparatory sequences listed in Table 1. Each preparatory sequence provides a different net excitation profile over the expected range of offsets providing varying sensitivity to offsets between ω and ω_0.

Modeling the preparatory pulse sequences

To determine the sensitivity of each preparatory sequence to a range of offsets, the induced spin dynamics are modeled for a finite range of ω_0. We start with a uniform distribution of unit magnetizations oriented in the $+z$ direction, where each magnetization is assigned a different offset frequency. The effect of the first pulse is modeled: This involves the rotation of each magnetization about their B_{eff} axis (equation 4) through an effective flip angle, β_{eff}, described by equation 5 (Walbrecker et al., 2011):

$$\beta_{\text{eff}} = \sqrt{(\gamma B_1)^2 + (\Delta \omega)^2} \cdot \tau. \qquad (5)$$
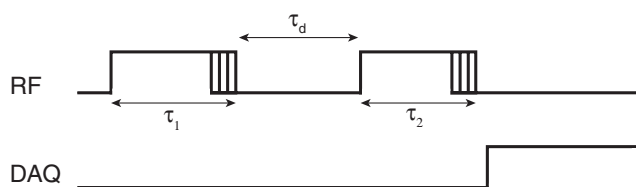

Figure 5. Timing diagram for the preparatory pulse sequences utilized in this study, each consisting of two individual B_1 radio-frequency (RF) pulses of length τ_1 and τ_2 separated by a delay time τ_d, and a mutual phase shift Φ. Timing parameters are varied for different sequences, indicated by the multiple vertical lines at the end of the pulses. Data acquisition (DAQ) represents the time when the receiver coil is off or on. Only the FID following the second pulse is recorded (DAQ on).

Table 1. Parameters defining the suite of preparatory pulse sequences.

PS index	Pulse 1 flip angle (°)	Dwell time, τ_D (μs)	Pulse 2 flip angle (°)	Phase difference Φ between pulses 1 and 2 (°)
1	30	3	80	180
2	45	20	45	0
3	40	50	50	270
4	45	50	45	180
5	70	50	70	90
6	90	100	90	270
7	90	100	90	180
8	50	50	70	180
9	40	50	130	90
10	40	50	130	270
11	90	100	50	180

Each magnetization n has a distinct $B_{\text{eff},n}$ axis and $\beta_{\text{eff},n}$ because of their unique $\Delta \omega_n$. After the first pulse, each magnetization's transverse component accumulates a phase ($\varphi = \Delta \omega_n \tau_d$) during the delay time τ_d. Next, the effect of the second pulse is modeled; each magnetization is again rotated about their unique $B_{\text{eff},n}$ axis, through an angle $\beta_{\text{eff},n}$. Because the delay time and the pulse durations are relatively short, we ignore the effect of relaxation during these times. Note that each magnetization is oriented differently prior to the second pulse, in contrast to case of the first pulse that encountered all magnetizations in their equilibrium position.

To forward model the predicted FID amplitude and phase, we calculate the final transverse magnetization following every preparatory sequence. All M_x and M_y components are stored in the kernel matrix $\mathbf{K}$ of dimension [2N, 2N], where N is the number of preparatory sequences. The final M_x and M_y components following the first preparatory sequence are stored in rows 1 and 2 of $\mathbf{K}$, respectively. The matrix $\mathbf{K}$ allows the predicted FID amplitude and phase (at time 0) following each preparatory sequence to be forward modeled given an arbitrary B_0 distribution using equation 6:

$$\mathbf{M} = \mathbf{KH}, \qquad (6)$$

where $\mathbf{H}$ is a vector of size [2N, 1] containing the amplitude of the B_0 distribution at each discrete offset.

Inversion to determine the statistical distribution of B_0

Using the measured variation in FID amplitude and phase following each preparatory sequence and the kernel matrix $\mathbf{K}$, a Levenberg-Marquadt inversion (Aster et al., 2005) is employed to estimate the statistical distribution of B_0. To ensure that the inverse problem is even determined, the result of the inversion is the vector $\mathbf{H}$ (equation 6) of size [2N, 1] containing the amplitude of the B_0
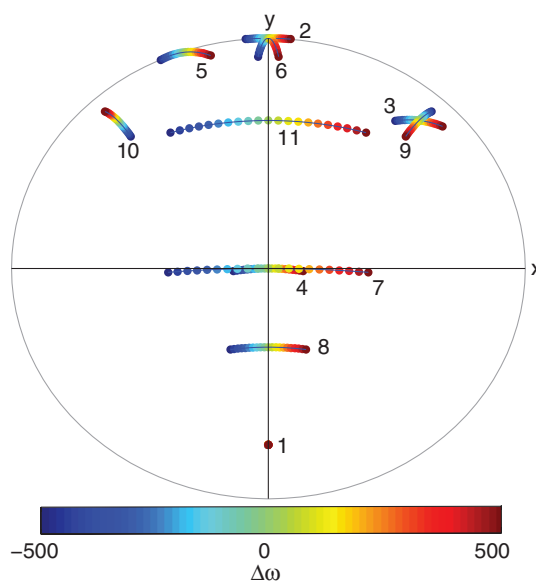

Figure 6. Transverse projection of the final magnetizations (circles) following the 11 preparatory sequences listed in Table 1 (corresponding numbers 1–11), for a range of offsets ± 500 Hz about ω (offset indicated by color). Preparatory sequence 1, which produces the same transverse magnetization for all offsets, is used for phase correction (see text for details).

distribution at $2N$ discrete offsets, as each FID has a real and quadrature component (equivalent to the M_y and M_x components, respectively). The inversion is constrained using information available from the Fourier transform (FT) of the measured FIDs of equation 3,

$$M(f) = M_0(H(f) \otimes L(f, T_2)), \qquad (7)$$

where $M(f)$ is the FT of $M(t)$, $L(f, T_2)$ is the Lorentzian obtained from the FT of the exponential T_2 decay, and $H(f)$ is the FT of $h(t)$. Note that $H(f)$ is the desired B_0 distribution (Yablonskiy and Haacke, 1994).

We do not need to explore all frequencies in the inversion. The model space may be restricted to a range of offsets no wider than the FT of the FID; the convolution of two functions, as represented by $M(t)$ in equation 7, is always wider than either of the constituting functions, $H(f)$ and $L(f, T_2)$ in equation 7. This greatly limits the range of offsets that must be examined in the inversion. A positivity constraint is also imposed in the inversion, as there cannot be fewer than zero spins at any given offset. An estimate for the upper bound of $H(f)$ is given by the maximum amplitude of $M(f)$, which is determined by the multiplication of the peaks of $H(f)$ and $L(f, T_{2i})$ during convolution. We implement as a hard upper bound a smooth function $A_{\max}(f)$, built to be roughly twice as large as the maximum of $M(f)$. This is done to limit the impact of the upper bound on the inversion result. To summarize the constraints imposed in the inversion: (1) $H(f)$ bandwidth restricted to width of $M(f)$; (2) positivity constraint $H(f) > 0$; (3) rough upper bound based on magnitude of $M(f)$, $H(f) < 2 * \max(M(f))$. These constraints greatly reduce the scope of the inversion, limiting the model space to a region contained between $A_{\max}(f)$ and zero over a finite region of offsets. The constraints are imposed in the inversion using a tangent transform described in detail in Lehmann-Horn et al. (2011).

Combining steps 1–3 offers the ability to predict the statistical distribution of B_0 using only NMR measurements, allowing us to isolate $H(f)$ in equation 7 by performing an inversion to decouple it from the $L(f, T_2)$ term in the FT of the FID. Important to note is that the inversion results in a statistical distribution of the magnitude of B_0, not the B_0 gradients as are predicted using the spin-echo (Hurlimann, 1998) and modified CPMG sequences (Sun and Dunn, 2002). These methods estimate B_0 inhomogeneity at the diffusion length scale; the estimated gradient is the variation in B_0 divided by the diffusion length scale. In contrast, our method directly estimates the B_0 variation decoupled from a length scale, as we assume a regime where the length scale of B_0 inhomogeneity is greater than the diffusion scale. As we are interested in addressing the dephasing present in FID measurements, it is essential to quantify the magnitude.

Estimating the impact of B_0 inhomogeneity on T_2*

To quantify the discrepancy between T_2* and T_2, we use the estimated statistical distribution of B_0 and equations 3 and 7 to account for the impact of B_0 inhomogeneity on the FID. The distribution $H(f)$ is first interpolated onto a finer frequency discretization. Interpolation is performed in the frequency domain to allow $h(t)$ to be predicted to longer times in an attempt to ensure that the periodic nature of the discrete Fourier transform does not influence the initial decay. This finer discretization is not used in the inversion to predict $\mathbf{H}$ to limit the number of preparatory sequences,

and to ensure the inverse problem remains even determined. The Fourier transform of the interpolated $H(f)$ is taken to quantify the dephasing function $h(t)$ (equation 3). Next, the dephasing function is normalized, $h(0) = 1$. This is necessary because dephasing can only attenuate the signal not amplify it. The FID is then divided by the dephasing function $h(t)$ at each time point resulting in a predicted decay free of the effect of B_0 inhomogeneity.

At later times where the FID has appreciably decayed, signal-to-noise ratio (S/N) deteriorates, introducing additional noise into the estimate of the relaxation times of this predicted decay. Therefore, the decay is truncated using a cutoff time and only the decay prior to this cutoff time is inverted to estimate the underlying distribution of relaxation times (Whittall and Mackay, 1989). The resultant relaxation times are referred to in this paper as the *predicted* T_2. They represent our attempt to compensate for the impact of B_0 inhomogeneity on T_2*, to subsequently predict the decay that would have occurred given a homogeneous B_0.

Examination of the FID to determine when the predicted decay begins to deteriorate can be used to set the cutoff time. We recommend using $2T_2*$ as an upper limit on the cutoff time because the FID will be very attenuated after this time ($<14\%$ original amplitude). It is also suggested to not use cutoff times shorter than $T_2*/2$ to ensure a long enough time series for adequate resolution of the relaxation times during the inverse Laplace transform.

RESULTS AND MEASUREMENTS

Numerical study

Synthetic results serve to demonstrate that (1) FIDs measured after the suite of preparatory sequences listed in Table 1 may be used to provide insight into the B_0 inhomogeneity and (2) the robustness of the inversion to predict a range of plausible B_0 distributions.

To generate synthetic data, the induced spin dynamics during each preparatory sequence listed in Table 1 were modeled to build the kernel matrix $\mathbf{K}$. Combined with a predetermined B_0 distribution ($\mathbf{H}$), equation 6 is used to model the predicted FID amplitude and phase following each preparatory sequence; after forward modeling, 20% Gaussian noise is added to all synthetic data. To verify the accuracy of the developed inversion, its robustness was tested using a variety of synthetic data sets investigating the ability to reproduce a wide range of B_0 distributions, the effect of the initial model and impact of the upper bounds. Figure 7a demonstrates that the inversion is able to accurately reproduce Lorentzian B_0 distributions of varying widths, where the predicted B_0 distributions (dashed lines) closely reproduce the true distributions (solid lines). Aside from imposing a regularization that provides a smooth solution, no assumptions regarding the shape of the B_0 distribution are implemented in the inversion; we also tested the procedure successfully on Gaussian and square B_0 distributions. Implementation of the upper and lower bounds greatly improves the performance of the inversion as demonstrated in Figure 7b, where the performance of an unconstrained and constrained inversion are compared for the same data and initial model. The unconstrained inversion (blue line) fails to reproduce the shape of the underlying B_0 distribution (black line), requiring unphysical negative amplitudes to fit the data. In contrast, the constrained inversion (red line) is able to accurately predict the B_0 distribution. The inversion also does not display large sensitivity to either the choice of initial model or upper bounds; as

long as the upper bound is chosen generously enough to ensure that the final model is not of similar magnitude to the upper bound.

Doped water samples

To verify the feasibility of the methodology, we conducted a controlled laboratory experiment where the B_0 inhomogeneity is due to imperfections in the field generated by the permanent magnet geometry in the core analyzer. Three water samples containing 10mL of deionized water were doped with 0.0184 g (sample 1), 0.1234 g (sample 2), and 0.4715 g (sample 3) of $FeSO_4$, respectively. Controlling the $FeSO_4$ concentration provides a means to control the T_2 of each sample. Using a 2.2 MHz NMR core analyzer, we measured (1) the FID amplitude and phase after each preparatory sequence listed in Table 1, (2) an FID following a single $\pi/2$ pulse, and (3) the T_2 decay using a CPMG pulse sequence as reference. The measured FID and CPMG for all three samples are shown in Figure 8a and 8c, respectively.

The relaxation time distribution underlying each curve was determined using an inverse Laplace transform (Whittall and Mackay, 1989); results are displayed in Figure 8b (for T_2*) and Figure 8d (for T_2). The T_2* distributions cluster together at early times, whereas the T_2 distributions for each sample are well separated on the relaxation time axis. The similar FIDs and distinct T_2 suggest that dephasing associated with B_0 inhomogeneity (T_{2IH}) plays the dominant role in the FID.

Prior to inversion, to determine the statistical distribution of B_0, a phase correction Φ_{cor} is applied to all FIDs measured after each preparatory sequence. This is necessary as only the relative phases of the two individual pulses may be controlled experimentally, while the modeling to build **K** contains an implicit assumption that the absolute phase is zero for the first pulse in every preparatory sequence. The phase correction Φ_{cor} is determined from the first preparatory sequence in Table 1 ($30_x - 3 \mu s - 80_{-x}$). Figure 6 demonstrates that this particular pulse (labeled #1) uniformly excites the entire investigated region of offsets to have an entirely negatively real component ($-y$ component) provided an absolute phase of zero for the first pulse. Therefore, Φ_{cor} is determined by ensuring this particular FID has only a negative real component.

To constrain the inversion for **H**, we examine the FT of the FID for each sample (red line in Figure 9a, 9c, and 9e). We restrict our model space to a range of offsets ± 500 Hz of ω because no FID displays a bandwidth greater than ~1 kHz. Upper bounds chosen to be roughly twice the peak of the FT FID were implemented as quadratic functions of maximum ~2000, 1800, and 1000 for samples 1, 2, and 3, respectively. For each sample, the measured FID amplitudes and phases were inverted to estimate the statistical distribution of B_0, shown in Figure 9a, 9c, and 9e (black lines). Figure 9b, 9d, and 9f demonstrates the ability to predict the observed variation in FID amplitude and phase given the predicted B_0 distributions. Data misfits are visualized as deviation from the 1:1 line; the FID amplitudes and phases are accurately predicted given the estimated B_0 distributions for all samples.

We now use our estimate of the B_0 distribution to test our hypothesis that the impact of B_0 inhomogeneity on T_2* can be estimated given the statistical distribution of B_0. For each sample, the component of the FID due to B_0 inhomogeneity is estimated, and a predicted decay formed. Each decay was truncated at three different cutoff times, and the underlying relaxation-time distributions predicted (referred to as predicted T_2 in Figure 10a–10c for samples 1–3, respectively). Cutoff times of $T_2*/2$ (dotted red line), T_2* (solid red line), and $2T_2*$ (dashed red line) were used in samples 1 and 3. For sample 2, the chosen cutoff times were the time when FID reached 50% its initial amplitude, T_2*, and $2T_2*$. The time $T_2*/2$ was not used in this case because the predicted decay increased at very early times. If $h(t)$ decays too quickly compared to the FID, noise can cause the predicted decay to initially increase, which is unphysical.

The impact of B_0 inhomogeneity on the FID is accurately estimated for samples 2 and 3 using all cutoff times, as evidenced by the good agreement between the predicted and true T_2. Sample 1's predicted T_2 distribution varied greatly depending on the cutoff time, and did not reproduce the true T_2 accurately. Table 2 summarizes the results listing the mean log of the T_2*, true T_2, and predicted T_2 using a cutoff time of T_2*. For samples 2 and 3, where
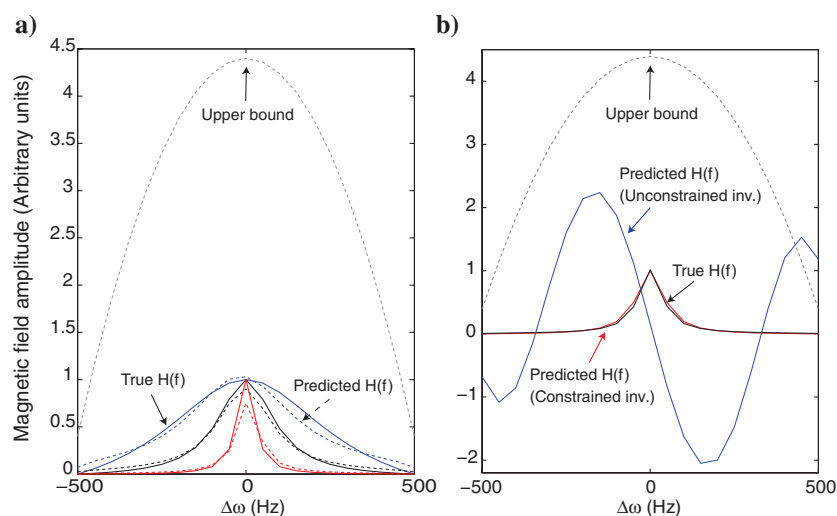

Figure 7. (a) Constrained-inversion results for three different B_0 distributions (colors); predicted and true B_0 distributions are shown in dashed and solid lines, respectively. The dashed gray line depicts the upper amplitude constraint in inversion. (b) Comparison of results for constrained (red line) and unconstrained (blue line) inversions to reproduce the true B_0 distribution (black line). The dashed gray line depicts the upper amplitude constraint in inversion.

Table 2. Mean log of the T_2*, true T_2, and predicted T_2 distributions for the doped water samples.

	Sample 1	Sample 2	Sample 3
T_2* mean log (ms)	7.1	5.5	2.8
True T_{2ML} (ms)	261.9	26.7	3.8
Predicted T_{2ML} for cutoff time of T_2* (ms)	19.6	30.7	3.8

good agreement is observed between the predicted and true T_2, the cutoff time was empirically optimized (5.7 ms and 5 ms for samples 2 and 3, respectively) and the resulting predicted T_2 distributions shown in Figure 11.

Figure 8. (a) The T_2* decay and (b) T_2* distribution after a single $\pi/2$ pulse for doped water samples with 0.0184 g (sample 1; red), 0.1234 g (sample 2; blue), and 0.4715 g (sample 3; black) of $FeSO_4$ dissolved in 10 mL of deionized water. (c) The T_2 determined by CPMG and (d) T_2 distributions for the samples in (a). Note the different time scales in (a) and (c).

Figure 9. (a, c, e) Comparison between the Fourier transform of the measured FID (red line) and the predicted B_0 distribution (black line) for samples 1, 2, and 3, respectively. (b, d, f) Measured and predicted complex FID amplitudes following the 11 preparatory sequences (Table 1) for the doped water samples 1, 2 and 3, respectively. Predictions are based on the B_0 distributions shown in (a, c, e). The solid line indicates the one-to-one line. Squares and circles indicate the real and quadrature components of the FIDs, respectively.

DISCUSSION

A novel technique is developed to encode information about the characteristics of the B_0 distribution in the amplitude and phase of FIDs following preparatory sequences. Results of our numerical study verify the ability to predict the statistical distribution of B_0 from the measured FID amplitude and phase following each of the preparatory sequences listed in Table 1. A proof of concept was performed in a controlled laboratory setting using several doped water samples. The predicted B_0 distributions for all three doped water samples (Figure 9) were very similar. This consistency further demonstrates the robustness of the developed inversion. The source of B_0 inhomogeneity in each case is the natural inhomogeneity in the field created by the geometry of the permanent magnets in core analyzer. As such, each sample is subject to the same variation in B_0 and the consistent estimates are evidence for the reliability of the method. The developed methodology is a novel technique providing estimates of the statistical distribution of B_0, and a step toward improving our ability to account for the effects of B_0 inhomogeneity on T_2* data. Knowledge of B_0 inhomogeneity may also give qualitative insight into the type of materials present: for example, examining the width of the B_0 distribution may identify high or low susceptibility materials.

Given that the developed methodology provides the ability to robustly estimate the statistical distribution of B_0, we next test the hypothesis that the impact of B_0 inhomogeneity on T_2* can be quantified using our estimate of the B_0 distribution. We compare T_2 distributions from (1) a CPMG pulse sequence that compensates for B_0 inhomogeneity (true T_2) and (2) our methodology to compensate for the impact of B_0 inhomogeneity on the FID (predicted T_2). In situations where there are moderate (within an order of magnitude) differences between T_2* and T_2 (samples 2 and 3), the cutoff time did not introduce significant uncertainty in the predicted T_2 distributions. This is a regime not uncommon in earth's field measurements where long T_2* (50 ms to a few hundred ms) are often observed. In these cases, knowledge of the B_0 distribution may provide the ability to accurately quantify the discrepancy between T_2* and T_2 increasing the utility of FID measurements for the estimation of pore-scale properties. In contrast, a potential limit is identified in sample 1 where the discrepancy between T_2* and T_2 is nearly two orders of magnitude; T_{2IH} overwhelmingly dominates the FID causing T_2* to carry little dependence on T_2. We conclude that any predictions of T_2 from T_2* will be unreliable for this sample because of the large sensitivity to the cutoff time. This regime is likely to be encountered only in strong B_0 fields
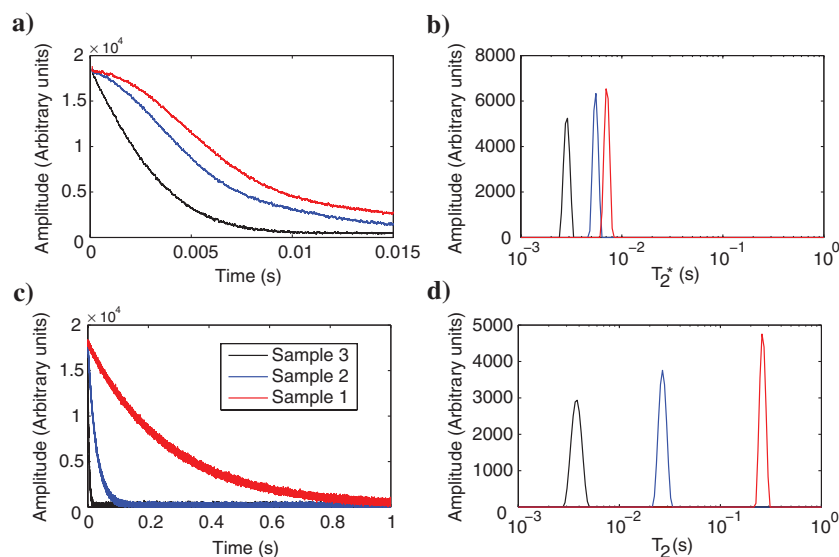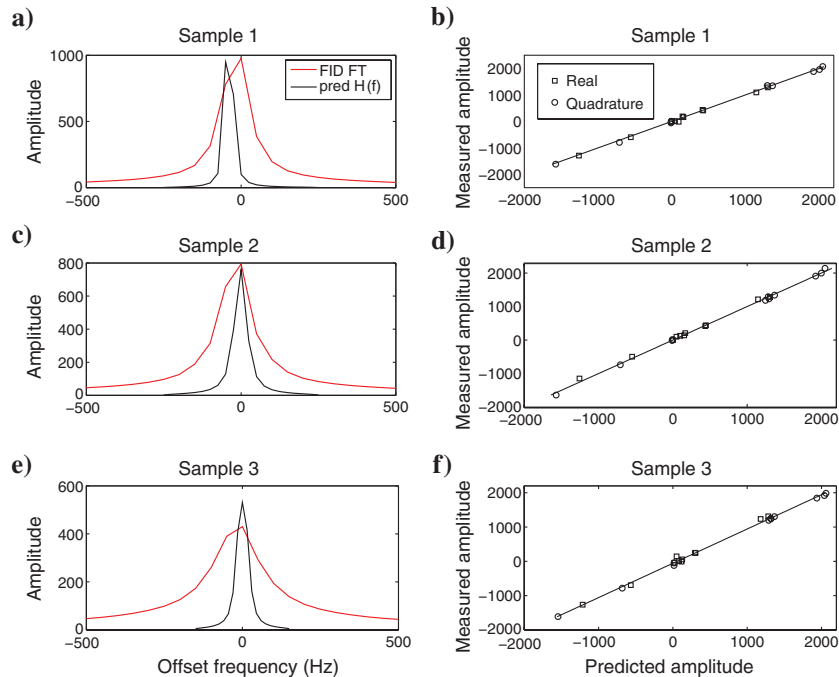
or highly magnetic materials. Part of the uncertainty in this case may also originate from the lack of resolution at these long predicted T_2 values. Several porous media samples were also tested, including glass beads and fine sands, but it was observed using our experimental setup (2.2 MHz B_0 field) that T_{2*} in these samples was several orders of magnitude smaller than T_2, similar to the case of sample 1. This is not expected to be a limitation of the methodology, but rather a consequence of working in a high B_0 field. We anticipate that in a weaker B_0 field porous media samples will be more likely to fall in a regime similar to samples 2 and 3 where T_{2*} is not drastically smaller than T_2 and the FID component due to B_0 inhomogeneity can be accurately estimated.

As a general guideline, we recommend using T_{2*} as the cutoff time, but further development in the selection of the appropriate cutoff time is needed. This is demonstrated in Figure 11, where the empirically optimized cutoff times provide very good results. As the true T_2 distribution will be unknown in practice, a technique to optimize the cutoff time based entirely on the FID measurement is needed. In practice, several cutoff times, in addition to a cutoff time of T_{2*}, should be used to investigate the uncertainty in the predicted T_2 distribution.

The particular preparatory sequences used in this study are not unique. Table 1 consists of a subset from a much larger collection of tested sequences, chosen based on their ability to provide distinct footprints in the transverse plane (Figure 6). A comprehensive analysis to optimize the number of preparatory sequences and the particular combination of flip angles, delay times, and relative phases has yet to be conducted; rather the suite used in this paper was designed as a proof of concept. To implement each preparatory sequence experimentally, the specific flip angles were obtained by modifying the pulse duration, not the B_1 amplitude. As pulse durations in this study are typically 15–25 µs, varying individual pulse lengths is not expected to impede the ability of each pulse to excite the entire range of offsets present. The pulse bandwidths (roughly 50 kHz), determined by $\tau_{1,2}$, are much wider than the anticipated range of offsets present.

Important to note is that no assumptions regarding B_0 shape are made during the current inversion. However, if assumptions regarding shape were implemented prior to inversion, the number of model parameters would be dramatically reduced. For example, instead of inverting for **H**, where there are $2N$ model parameters, fitting a Lorentzian or Gaussian to the B_0 distribution would require only three model parameters: the peak height, the width, and its center frequency. This type of strategy may considerably reduce the number of necessary preparatory sequences, potentially speeding up measurement times.

A technique that may benefit from this methodology is surface NMR. It presents an opportunity to potentially extract information about

pore-scale properties from the FID, a standard measurement in surface NMR, unbiased by the influence of B_0 inhomogeneity. However, prior to implementation in the field, several key differences between the controlled laboratory environment of this proof of concept study and surface NMR conditions must be addressed. The first regards the use of heterogeneous B_1 in surface NMR. This causes each individual pulse to apply flip angles that vary spatially, in contrast to the laboratory case where we can assume that each pulse applies a roughly uniform flip angle across the entire excited volume. As a result of the spatially varying flip angle, it will be necessary to have an estimate of the spatial distribution of the water content to accurately model the FID amplitude and phase following the preparatory pulse sequence. This information may be extracted from depth-profiling FID measurements, which will accompany the preparatory pulse sequence. Furthermore, as the preparatory pulses rely on the underlying B_0 distribution to produce FID amplitude and phase variation, it is likely that the method will perform best when the preparatory pulses target a single depth. This will reduce additional amplitude and phase variation that could arise in surface NMR if the pulse amplitudes were varied to sample different depths.
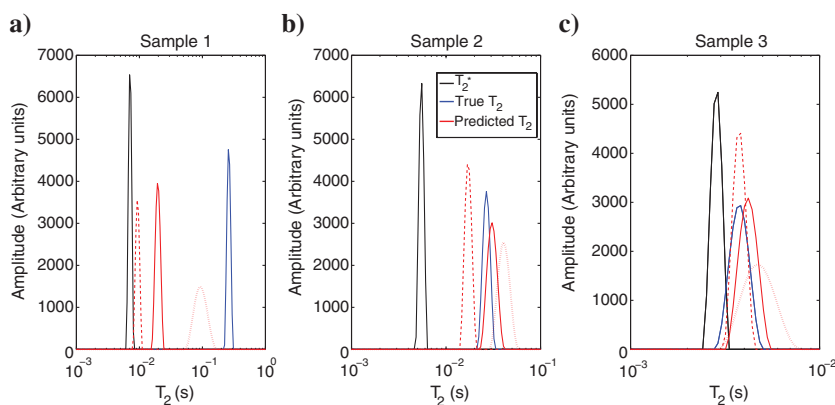

Figure 10. Ability of the developed methodology and FID measurements to predict the true T_2 distribution. (a, b, c) The T_{2*} (black), true T_2 (blue), and predicted T_2 (red) distributions for samples 1, 2, and 3, respectively. The predicted T_2 distributions are determined using cutoff times of $T_{2*}/2$ (dotted), T_{2*} (solid), and $2T_{2*}$ (dashed) in samples 1 and 3. The cutoff times used in sample 2 are T_{2*} (solid), $2T_{2*}$ (dashed), and the time when the FID reaches 50% its initial amplitude (dotted) as explained in the text. Note the different T_2 scales.
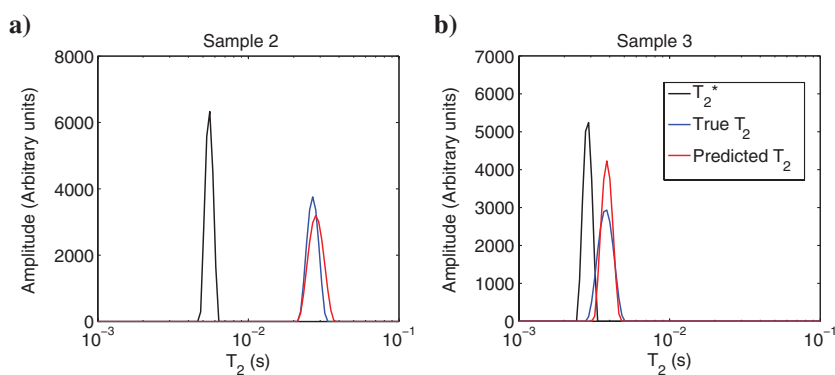

Figure 11. Distributions of T_{2*} (black), true T_2 (blue), and predicted T_2 (red) using the optimal cutoff times for samples 2 and 3, shown in (a) and (b), respectively. The optimal cutoff times were 5.7 ms and 5 ms for samples 2 and 3, respectively.

However, further work is required to investigate whether we retain the sensitivity to estimate the B_0 distribution in a heterogeneous B_1 experiment.

Another difference between surface NMR and the laboratory conditions of this study is the B_0 strength, ~2 kHz versus 2.2 MHz, respectively. The weaker field in surface NMR will result in narrower B_0 distributions (roughly <10–20 Hz wide), much narrower than the estimated distributions in Figure 9. As a result, dephasing will occur at a slower rate and the preparatory pulse sequences used in this study will need to be modified. The longer pulse durations used in surface NMR (~5–40 ms) will partially compensate for the slower dephasing rates, as they provide more time for the magnetizations to fan out, but it is likely that the delay time will also need to be increased to allow the magnetizations to further dephase. Weaker B_0 is also expected to increase the probability that the FID will be in a regime similar to samples 2 and 3, where T_2* is within an order of magnitude of T_2 and the methodology can provide accurate estimates of the influence of B_0 inhomogeneity.

Alternative data acquisition strategies currently employed in surface NMR, such as the pseudosaturation recovery or spin-echo pulse sequences, implicitly address the influence of B_0 inhomogeneity through direct T_1 or T_2 measurements. What these methods are able to do themselves, we aim to provide for the FID using preparatory pulse sequences as a complementary tool to quantify the influence of B_0 inhomogeneity on the FID measurement, effectively providing an external means to address a major concern in the FID measurement. The advantage in this strategy is that it allows the attractive features of the FID measurement, such as the high-density time sampling and ability to measure the fastest relaxation times, to be exploited. In contrast, the techniques to measure T_1 or T_2 directly provide the ability to alleviate the impact of B_0 inhomogeneity at the expense of a high-density time sampling (typically only sampling the decay at several delay times) and begin their measurements at a much later time after the initial excitation reducing their sensitivity to the fastest relaxation times.

CONCLUSIONS

NMR measurements of the FID curve provide estimates of the relaxation time T_2*, which can give insight into pore-scale properties of porous media. In many practical cases, however, this potential cannot be exploited because the FID is dominated by the effect of spatial variations in the background field B_0. To improve the usefulness of FID measurements for the estimation of pore-scale properties, we have developed a new methodology to estimate the statistical distribution of B_0 in an NMR experiment and remove its effect on the FID. The method involves inverting the measured FID amplitude and phase variation following a suite of preparatory pulse sequences to estimate the statistical distribution of B_0. Knowledge of the B_0 distribution provides the ability to account for the impact of B_0 inhomogeneity that occurs at a scale greater than the diffusion length scale, a necessity when dealing with FID measurements that have no ability to directly account for dephasing. We are able to demonstrate, in a controlled laboratory study on doped water samples, that knowledge of the statistical distribution of B_0 is sufficient to quantify the impact of B_0 inhomogeneity on the FID when the discrepancy between T_2* and T_2 is less than an order of magnitude. We conclude that the ability to estimate the statistical

distribution of B_0 makes it possible to quantify and correct for the impact of B_0 inhomogeneity on the FID.

Surface NMR is a technology that may stand to benefit from this type of approach. The preparatory pulse sequences require only two B_1 pulses. As such, hardware constraints that currently limit the implementation of sophisticated pulse sequences involving long pulse trains in surface NMR will not be a concern. This work is an important first step demonstrating the feasibility of a methodology motivated to address a concern in surface NMR FID measurements. It aims to offer a complementary tool to the FID that provides the ability to account for the impact of B_0 inhomogeneity on the FID measurement, which may mask other mechanisms influencing T_2*. As such, it offers the ability to investigate the other mechanisms impacting the FID that potentially contain valuable information about pore-scale properties. Although further work is required prior to implementation of this methodology in surface NMR, specifically to address conditions related to weaker B_0 and heterogeneous B_1, the preparatory pulse sequence method offers the potential to advance the use of the FID for estimation of pore-scale properties.

ACKNOWLEDGMENTS

REFERENCES

Aster, R. C., B. Borchers, and C. H. Thurber, 2005, Parameter estimation and inverse problems: Elsevier Academic Press.
Bloom, A. L., 1955, Nuclear induction in inhomogeneous fields: Physical Review, **98**, 1105–1111, doi: 10.1103/PhysRev.98.1105.
Brownstein, K. R., and C. E. Tarr, 1979, Importance of classical diffusion in NMR-studies of water in biological cells: Physical Review A, Third Series, **19**, no. 6, 2446–2453, doi: 10.1103/PhysRevA.19.2446.
Callaghan, P. T., 1991, Principles of nuclear magnetic resonance microscopy: Oxford University Press.
Carr, H. Y., and E. M. Purcell, 1954, Effects of diffusion on free precession in nuclear magnetic resonance experiments: Physical Review, **94**, no. 3, 630–638, doi: 10.1103/PhysRev.94.630.
Chen, Q., A. E. Marble, B. G. Colpitts, and B. J. Balcom, 2005, The internal magnetic field distribution, and single exponential magnetic resonance free induction decay, in rocks: Journal of Magnetic Resonance, **175**, 300–308, doi: 10.1016/j.jmr.2005.05.001.
Coates, G. R., R. C. A. Peveraro, A. Hardwick, and D. Robert, 1991, The magnetic resonance imaging log characterized by comparison with petrophysical properties and laboratory core data: Society of Petroleum Engineers, 22723-MS.
Cohen, M. H., and K. S. Mendelson, 1982, Nuclear magnetic-relaxation and the internal geometry of sedimentary-rocks: Journal of Applied Physics, **53**, 1127–1135, doi: 10.1063/1.330526.
Dlubac, K., R. Knight, Y. Song, N. Bachman, B. Grau, J. Cannia, and J. Williams, 2013, Use of NMR logging to obtain estimates of hydraulic conductivity in the High Plains aquifer, Nebraska, USA: Water Resources Research, **49**, 1871–1886, doi: 10.1002/wrcr.20151.
Freeman, R., S. P. Kempsell, and M. H. Levitt, 1980, Radio frequency pulse sequences which compensate their own imperfections: Journal of Magnetic Resonance, **38**, 453–479.
Godefroy, S., J. P. Korb, M. Fleury, and R. G. Bryant, 2001, Surface nuclear magnetic resonance and dynamics of water and oil in macroporous media: Physical Review E, **64**, 21605-1–21605-13, doi: 10.1103/PhysRevE.64.021605.
Grant, F. S., and G. F. West, 1965, Interpretation theory in applied geophysics: McGraw-Hill Book Co.

Grunewald, E., and R. Knight, 2011, The effect of pore size and magnetic susceptibility on the surface NMR relaxation parameter T2*: Near Surface Geophysics, **9**, 169–178, doi: 10.3997/1873-0604.2010062.

Grunewald, E., and R. Knight, 2012, Non-exponential decay of the surface-NMR signal and implications for water content estimation: Geophysics, **77**, no. 1, EN1–EN9, doi: 10.1190/geo2011-0160.1.

Hahn, E. L., 1950, Spin echoes: Physical Review, **80**, no. 4, 580–594, doi: 10.1103/PhysRev.80.580.

Hurlimann, M. D., 1998, Effective gradients in porous media due to susceptibility contrast: Journal of Magnetic Resonance, **131**, 232–240, doi: 10.1006/jmre.1998.1364.

Kenyon, W., P. Day, C. Straley, and J. Willemsen, 1988, A three-part study of NMR longitudinal relaxation properties of water-saturated sandstones, Society of Petroleum Engineers, 15643-PA.

Legchenko, A., and P. Valla, 2002, A review of the basic principles for proton magnetic resonance sounding measurements: Journal of Applied Geophysics, **50**, 3–19, doi: 10.1016/S0926-9851(02)00127-1.

Legchenko, A. V., and O. A. Shushakov, 1998, Inversion of surface NMR data: Geophysics, **63**, 75–84, doi: 10.1190/1.1444329.

Lehmann-Horn, A., J. O. Walbrecker, M. Hertrich, G. Langston, A. F. McClymont, and A. G. Green, 2011, Imaging groundwater beneath a rugged proglacial moraine: Geophysics, **76**, no. 5, B165–B172, doi: 10.1190/geo2011-0095.1.

Levitt, M. H., 1986, Composite pulses: Progress in Nuclear Magnetic Resonance Spectroscopy, **18**, 61–122, doi: 10.1016/0079-6565(86)80005-X.

Levitt, M. H., 2006, Spin dynamics: Basics of nuclear magnetic resonance: John Wiley and Sons Ltd.

Meiboom, S., and D. Gill, 1958, Modified spin-echo method for measuring nuclear relaxation times: Review of Scientific Instruments, **29**, no. 8, 688–691, doi: 10.1063/1.1716296.

Muller, M., S. Kooman, and U. Yaramanci, 2005, Nuclear magnetic resonance (NMR) properties of unconsolidated sediments in field and laboratory: Near Surface Geophysics, **3**, 275–285.

Plata, J., and F. Rubio, 2008, The use of MRS in the determination of hydraulic transmissivity: The case of alluvial aquifers: Journal of Applied Geophysics, **66**, 128–139, doi: 10.1016/j.jappgeo.2008.04.001.

Roy, J., A. Rouleau, M. Chouteau, and M. Bureau, 2008, Widespread occurrence of aquifers currently undetectable with the MRS technique in Grenville geological province, Canada: Journal of Applied Geophysics, **66**, 82–93, doi: 10.1016/j.jappgeo.2008.04.006.

Seevers, D. O., 1966, A nuclear magnetic method for determining the permeability of sandstones: SPWLA Transactions, **7**, Paper L.

Slichter, C. P., 1980, Principles of magnetic resonance: Springer-Verlag.

Sun, B., and K. J. Dunn, 2002, Probing the internal field gradients of porous media: Physical Review E, **65**, 5, doi: 10.1103/PhysRevE.65.051309.

Timur, A., 1968, An investigation of permeability, porosity, and residual water saturation relationships: Annual SPWLA Symposium, 1968-J.

Walbrecker, J. O., M. Hertrich, and A. G. Green, 2011, Off-resonance effects in surface nuclear magnetic resonance: Geophysics, **76**, no. 2, G1–G12, doi: 10.1190/1.3535414.

Walsh, D., P. Turner, E. Grunewald, H. Zhang, J. J. Butler, E. Reboulet, S. Knobbe, T. Christy, J. Lane, C. Johnson, T. Munday, and A. Fitzpatrick, 2013, A small-diameter NMR logging tool for groundwater investigations: Ground Water, 1–13, doi: 10.1111/gwat.12024.

Whittall, K. P., and A. L. Mackay, 1989, Quantitative interpretation of NMR relaxation data: Journal of Magnetic Resonance, **84**, 134–152, doi: 10.1016/0022-2364(89)90011-5.

Yablonskiy, D. A., and E. M. Haacke, 1994, Theory of NMR signal behavior in magnetically inhomogeneous tissues — The static dephasing regime: Magnetic Resonance in Medicine, **32**, no. 6, 749–763, doi: 10.1002/mrm.1910320610.